frontiers in Materials

ORIGINAL RESEARCH
published: 19 November 2020
doi: 10.3389/fmats.2020.567130

Removal of Congo Red From Aqueous Solutions at Hardened Cement Paste Surfaces

Matthias Wagner[1]*, *Christina Eicheler*[1], *Brigitte Helmreich*[2], *Harald Hilbig*[1] and *Detlef Heinz*[1]

[1]Chair of Mineral Engineering, Technical University of Munich, Munich, Germany, [2]Chair of Urban Water Systems Engineering, Technical University of Munich, Munich, Germany

The removal of azo dyes is a critical issue in current textile industry wastewater treatment. In contemporary wastewater management, many structures that are in direct contact with wastewater are constructed with concrete. In this contribution, the removal of Congo red from aqueous solutions by the material in the surface of hardened binder paste was studied in multiple exposure experiments. Flat prisms made with ordinary Portland cement and ground granulated blast-furnace slag were stored in different aqueous solutions. The powdered surface material of these flat prisms was used as a substrate for the removal of Congo red from aqueous solutions. Storage in sodium sulfate solution lead to the formation of hydrotalcite nanosheets on the surfaces of hardened binder pastes rich in magnesium provided by the granulated blast-furnace slag. These nanosheets resulted in a large specific surface area and increased the discoloration capacity with respect to binder mass. The results also suggest that the carbonation of C-S-H can provide fresh calcite that can act as a secondary adsorbent. The results of this study suggest that cementitious binders with high magnesium contents could contribute to the removal of azo dyes from industrial wastewater by providing economically attractive treatment materials.

Keywords: azo dye, Congo red, cementitious binder, hardened cement paste, concrete, industrial wastewater

OPEN ACCESS

Edited by:
Antonio Caggiano, Darmstadt University of Technology, Germany

Reviewed by:
Martin Palou, Slovak Academy of Sciences (SAS), Slovakia
Marija Nedeljkovic, Delft University of Technology, Netherlands

***Correspondence:**
Matthias Wagner
ma.wagner@tum.de

Speciality section:
This article was submitted to Structural Materials, a section of the journal Frontiers in Materials

Received: *29 May 2020*
Accepted: *23 September 2020*
Published: *19 November 2020*

Citation:
Wagner M, Eicheler C, Helmreich B, Hilbig H and Heinz D (2020) Removal of Congo Red From Aqueous Solutions at Hardened Cement Paste Surfaces. Front. Mater. 7:567130. doi: 10.3389/fmats.2020.567130

1 INTRODUCTION

Synthetic dyes are commonly used in textile, cosmetics and other industries. An important group of them are azo dyes in textile industry (Van der Zee et al., 2001). The release of colored wastewater to the environment exhibits a significant impact on aquatic ecosystems, soil, air and the health of human beings (Weisburger, 2002; Kant, 2012; Sarayu and Sandhya, 2012). While in most industrialized countries the governmental legislation is becoming more stringent regarding the removal of dyes from textile industry effluents, in most developing and newly industrialized countries, e.g., Pakistan or India, wastewater effluents from textile industry became the main source of pollution of the environment (Kant, 2012; Sarayu and Sandhya, 2012; Imtiazuddin, 2018). Furthermore, with an increased demand for textile products worldwide, there is an increase in production volume of the textile industry and its wastewater proportionally, making it one of the main sources of severe pollution worldwide (Sarayu and Sandhya, 2012). Therefore, dye removal from textile industry wastewater has become a significant challenge over the past decades, and up to now, there is no single and economically attractive treatment method that can effectively decolorize industrial wastewater (Sarayu and Sandhya, 2012). The present contribution would like to contribute to the improvement of this environmental problem.

The color of azo dyes is caused by the chromophore group (-N=N-) (Dos Santos et al., 2007). The azo group is linked with two stable complex aromatic rings, which makes it difficult to decompose (Dos Santos et al., 2007). A number of wastewater treatment technologies such as adsorption, aerobic, and anaerobic biological degradation, electrochemical coagulation, photocatalytic decolorization, membrane distillation, and electrochemical oxidation have been investigated (e.g., Banat et al., 1996; Georgiou and Aivasidis, 2006; Dos Santos et al., 2007; Mohan et al., 2007; Sarayu and Sandhya, 2012; Lin et al., 2015; Li et al., 2017; Adeleke et al., 2018; Saleh and Taufik, 2019; Shetti et al., 2019). However, they are usually associated with high costs or low operational stability in industrial applications. For example, the traditional bio-degradation in wastewater treatment plants is impossible because of the stable complex aromatic rings (Wang et al., 2007; Sarayu and Sandhya, 2012). Membrane distillation, a thermal, membrane-based separation process, is a very effective method to remove dyes up to a high purity (Lin et al., 2015). Nevertheless, one of the main reasons for the limited usability of membrane distillation is the deterioration of membrane functions caused by membrane fouling and wetting problems that decrease the performance and therefore increase the operational costs (Lin et al., 2015). The industrial application of membrane distillation for dye removal is additionally limited due to its high energy consumption (Camacho et al., 2013). A promising method is also the application of multi-walled carbon nanotubes and their combination with magnetic spinel nickel ferrite as a magnetic photo catalyst for the effective removal of dye pollutants from aqueous environments (Zhu et al., 2015). However, there has been no application on a technical scale so far, nor is it to be expected that the materials will be readily available at reasonable costs in developing countries. In conclusion, there is still a need in the textile industry for affordable and readily available techniques or materials to remove azo dyes from industrial wastewater, especially in developing and newly industrialized countries.

The adsorption behavior of azo dyes on synthetic layered double hydroxides (LDH) was studied in recent years (Morimoto et al., 2011; Shan et al., 2015; Li et al., 2016; Zhang et al., 2017; Soltani et al., 2018). LDH phases occur in a large number of variations and can incorporate numerous bivalent and trivalent cations as well as several intercalated anions (Taylor, 1973; Mills et al., 2012). The interlayer anions can be exchanged for different anionic species and therefore LDH phases have attracted interest as agents for removing inorganic pollutants such as arsenic and selenite anions (Huang et al., 2015; Ma et al., 2018). In cementitious binders, different LDH phases occur frequently, e.g., monocarboaluminate (carbonate endmember of hydrocalumite, $Ca_4Al_2(OH)_{12}(CO_3) \cdot 5\ H_2O$), hemicarboaluminate ($Ca_4Al_2(OH)_{13}(CO_3)_{0.5} \cdot 5.5\ H_2O$), monosulfoaluminate (kuzelite, $Ca_4Al_2(OH)_{12}(SO_4) \cdot 6\ H_2O$), Friedel's salt (the chloride endmember of hydrocalumite, $Ca_4Al_2(OH)_{12}Cl_2 \cdot 4\ H_2O$) and hydrotalcite ($Mg_6Al_2(OH)_{16}(CO_3) \cdot 4\ H_2O$) (Matschei et al., 2007).

The occurrence and amounts of LDH phases in hardened cement paste are affected by binder composition. For example, an increased magnesium content due to the use of dolomite (Machner et al., 2018a) or ground granulated blast-furnace slag (GGBS) can increase the amount of hydrotalcite in the hardened cement paste (Gong and White, 2016); (Walkley et al., 2017). The exact composition of the LDH phases formed as well as the composition of other hydrate phases depends on the chemical composition of the GGBS used (Gong and White, 2016). In cementitious binders, GGBS is widely used as a substitute for Portland cement for economic and ecological reasons (Habert et al., 2010). Binders containing GGBS often exhibit an enhanced physical resistance to chemically aggressive solutions and their effect on concrete durability has been comprehensively studied in recent decades (Juenger and Siddique, 2015). Increasing attention has been paid to LDH phases concerning their suitability in catalysis and pollutant adsorption (Yang et al., 2016; Tichit et al., 1995; Debecker et al., 2009; Mohapatra and Parida, 2016). Also, calcium silicate hydrate phases (C-S-H) that are the main strength giving component of hardened Portland cement pastes have been assessed as a carrier material for active pharmaceutical substances (Zhu and Sham, 2014). Recent results also showed that GGBS-based cementitious binders loaded with Fe_2O_3, or TiO_2 can be utilized in the photocatalytic degradation of Congo red (Zhang et al., 2013) or even water (Zhang and Chai, 2014).

This leads to the research question of how the surface of hardened cement paste interacts with organic substances dissolved in aqueous solutions since many structures for water storage, drainage systems and wastewater treatment have cementitious surfaces. This study considers the phases that formed in the outermost surface layer of hydrated cementitious binders that are submerged in aqueous solutions of different chemical compositions and how the binder surface and its constituent phases interact with aqueous solutions of azo dye. It is particularly important that in developing and newly industrialized countries, where removal methods for dyes are most frequently required and used, the costs for the treatment must be kept as low as possible and all necessary materials should be widely available. Hardened cement paste could be one of these materials. As an example for azo dyes, Congo red (Disodium-3,3'[[1,1-biphenyl]-4,4'-diyl(bis(azo)]bis(4-aminonaphthalin-1-sulfonate)) is used in the current study since it is well established as a model substance for organic pollutants. Congo red is an asymmetric, sulfonated azo dye, belongs to the class of protein-binding dyes and has the power to cause anaphylactic shocks or cancer (Shetti et al., 2019). Because of its functional groups, the color of Congo red solutions is pH-dependent.

The aim of this study is to understand the composition of the outermost concrete surface and its ability to remove organic pollutants at the example of Congo red from the contact solution, which could be a step towards solving the micropollutant problem by tailoring binders to the individual needs of wastewater treatment plants.

2 MATERIALS AND METHODS

2.1 Binder Preparation and Initial Storage

Flat prisms (10 mm × 40 mm × 160 mm) of hardened cement paste were prepared using a Portland cement CEM I 42.5 R

(OPC) and ground GGBS. The chemical composition of the binder materials is shown in **Table 1** and the mineralogical composition of the OPC is in **Table 2**. No crystalline phases were detected in the GGBS. The water to binder ratio w/b was 0.5 (deionized water) for all samples and the pastes were prepared in a vacuum mixer to minimize air inclusions in the hardened cement paste. The amount of GGBS within the binder was varied from 18 wt% (non-standard cement, used here to study the effect of small GGBS proportions), 65 wt% (upper limit of CEM III/A, DIN EN 197-1) to 80 wt% (upper limit of CEM III/B, DIN EN 197-1) (DIN, 2011). The samples were demolded after 48 h to ensure a sufficient strength for flat prisms made with binders that contained 80 wt% GGBS. The flat prisms then were stored in saturated calcium hydroxide solution to an age of 28 days to increase the degree of hydration of the binder. Afterward, the samples were transferred to either sodium sulfate solution (30 gl^{-1} SO_4^{2-}) or saturated calcium hydroxide solution for at least 70 days at 20^{c}*irc*C. During this period, the storage solutions were renewed in 7 days intervals. The sample designation scheme denotes the amount of GGBS in the binder and the storage solution after the first 28 days. For example, sample "65_SO4" was prepared by using 65 wt% of GGBS and 35 wt% of OPC and then stored in sodium sulfate solution after the initial storage whereas sample "65_OH" was stored in saturated calcium hydroxide solution for the whole time.

2.2 Analytics

The mineralogical composition of the samples was analyzed using a θ-θ configuration (Bruker D8 Advance, CuKα radiation (λ = 1.54 Å), 40 kV, 40 mA) with a silicon strip detector (LynxEye XE-T) and an automatic divergence slit. The raw materials were ground in isopropanol to a grain size of <32 μm using a ball mill and then prepared in standard polymer holders by front-loading. The powdered samples after dye exposure experiments were ground dry in an agate mortar and placed on a silicon zero background sample holder. The diffractograms were recorded over a range of 5° to 70° 2θ in steps of 0.02° 2θ with a duration of 0.2 s per step. The chemical composition of the initial materials was determined using inductively coupled plasma optical emission spectroscopy (ICP-OES, Horiba Jobin Yvon Ultima 2) after digestion with hydrochloric acid. The N_2-BET specific surface area was measured using a MicrotracBEL Belsorp mini II. The samples for N_2-adsorption were dried at 40^{c}*irc*C in vacuum to minimize the impact of the drying on the samples composition. A scanning electron microscope (SEM, Hitachi FlexSEM 1000, tungsten filament cathode, SE detection, 3.0–15.0 kV, no sputter coating) was used in variable pressure mode at 30 Pa for imaging and energy dispersive X-ray spectroscopy (EDS, Oxford Instruments AZtecOne 30 mm^2, 15.0 kV) with element mapping on flat prism surfaces after their storage in sodium sulfate solution. The hydration of the flat prisms was stopped using isopropanol. A field emission scanning electron microscope (JEOL JSM-7500F, SE detection, 1.0 kV, no sputter coating) was used for high resolution imaging.

2.3 Azo Dye Exposure Experiments

For the batch experiments the top 200 μm layer of each flat prism surface was carefully removed with a spatula following storage in sodium sulfate solution or calcium hydroxide solution. The resulting powder was added to 10 ml of Congo red solution (100 mg L^{-1} dye) in a snap-on lid vial while stirring at 150 rpm at 20^{c}*irc*C. The Congo red solution was prepared by dissolving Congo red (sodium salt, Carl Roth GmbH + Co. KG) in deionized water. The mass of the hardened cement paste powder was adjusted for every mixture to obtain the same N_2-BET surface area of 0.68 m^2. The removal of Congo red from the aqueous solution was measured by UV/Vis photometry. For the measurement 5 ml dye solution was separated from the suspension by centrifuging at 6,000 rpm for 10 min. 4 ml of the dye solution from the centrifuge were then pipetted into a glass cuvette and after measuring the pH the extinction was measured at wavelengths of λ= 498 nm, 340 and 275 nm using a Dr. Lange Cadas 100 photometer. The residual solids and solutions were all returned to the vial after each measurement. These measurements were conducted after exposing the powder to the dye for periods of 30 min, 1, 3 or 4, 5 or 6, and 7 days. The initial pH of the Congo red solution was between 9.5 and 10.0, a range in which the adsorption of Congo red on hydrotalcite-like LDH phases is not affected by small changes in pH (Shan et al.,

TABLE 1 | Chemical composition of the binder components (ICP-OES, wt%).

	LOI	Na_2O	K_2O	CaO	MgO	Fe_2O_3	Al_2O_3	SiO_2
OPC	1.90	0.25	0.84	63.70	1.38	2.27	5.25	20.80
GGBS	0.40	0.35	0.43	40.06	6.65	1.04	12.46	36.41
	P_2O_5	SO_3	TiO_2	MnO	BaO	SrO	Cr_2O_3	—
OPC	0.26	2.78	0.28	0.06	0.05	0.21	0.03	—
GGBS	<0.01	2.12	0.55	0.59	0.10	0.05	0.10	—

TABLE 2 | Mineralogical composition of the CEM I 42.5 R (XRD (Rietveld), wt%, n.d.: not detected).

C3S	C2S	C3A	C4AF	Gypsum	Bassanite	Lime	Periclase	Quartz	Calcite
64	12	12	4	n.d.	3	n.d.	n.d.	<1	3

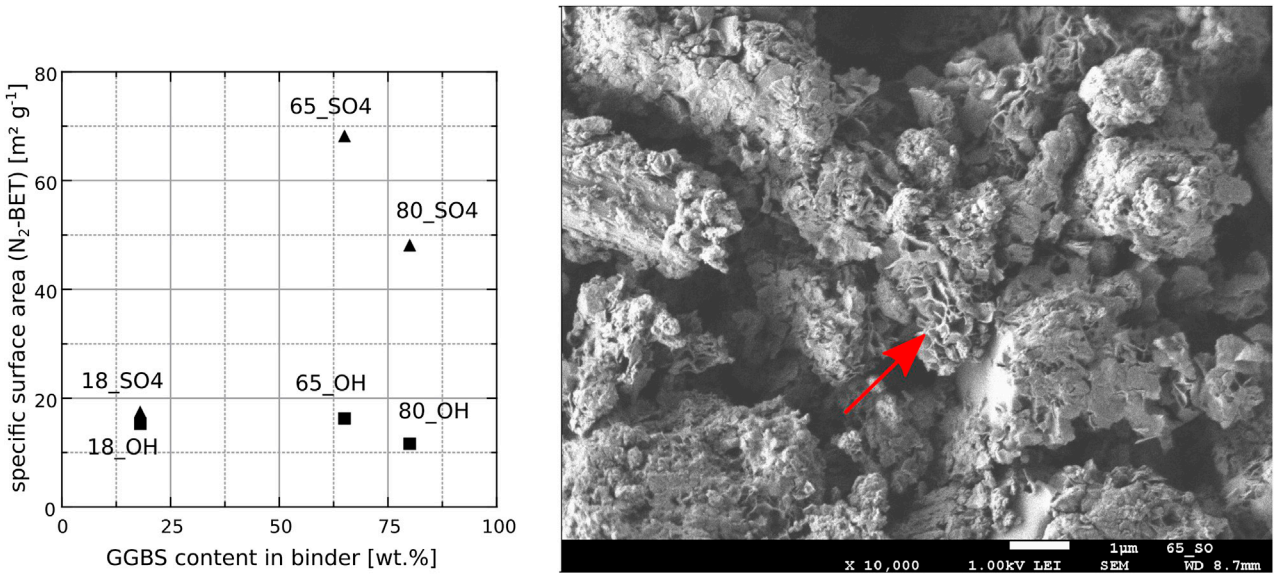

FIGURE 1 | Specific surface area (N_2-BET) of the surface layer of the hardened binder pastes **(left**; ■: stored in calcium hydroxide solution; ▲: stored in sodium sulfate solution). An increased specific surface area was observed for the binders with high GGBS contents following storage in sodium sulfate solution (65_SO4 and 80_SO4). Sheet-like structures rich in magnesium, most likely hydrotalcite, were observed by SEM on the surface **(right**, red arrow).

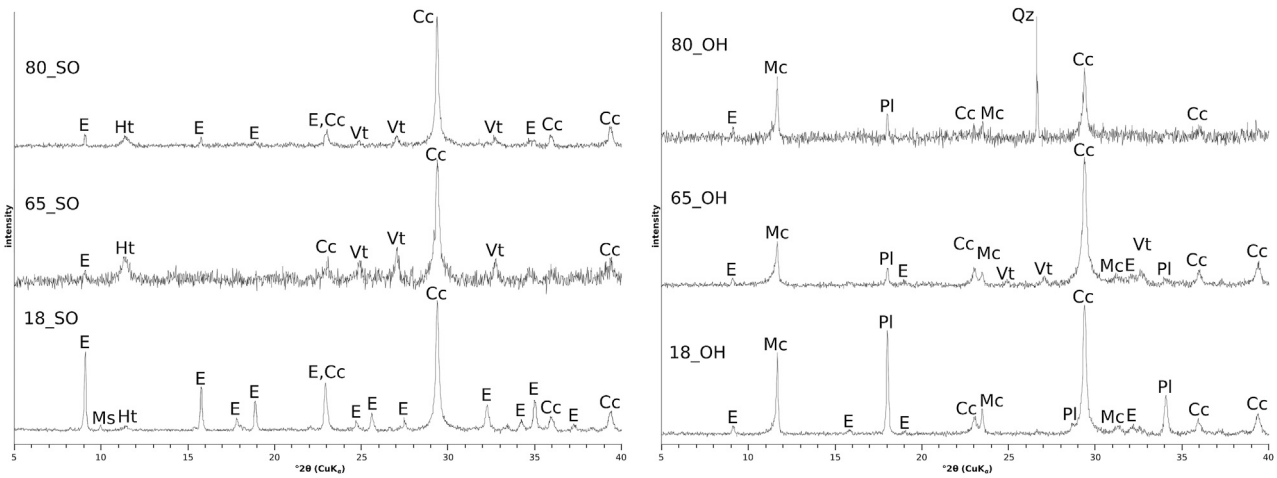

FIGURE 2 | X-ray diffractograms of the powdered surface layers of the hardened cement paste flat prisms after storage in sodium sulfate solution (30 gl^{-1} SO_4^{2-}, **left)** or in saturated calcium hydroxide solution **(right)**. E, ettringite; Cc, calcite; Ms, monosulfoaluminate; Ht, hydrotalcite; Vt, vaterite; Mc, monocarboaluminate; Pl, portlandite; Qz, quartz.

2015). A Congo red solution in deionized water was used as a reference. Following the last measurement, three subsequent exposure cycles were conducted with a duration of 7 days each. At the end of each cycle, the solids and Congo red solutions were separated by centrifuging and dried at room temperature. The solids were then added again to a fresh Congo red solution for the next exposure cycle. Analogous to the above experiments with hardened cement paste powders, Congo red exposure experiments were also carried out using phases that are typically observed in cementitious systems. Powdered activated carbon (AC) was used as a refrence material for dye adsorption since it is widely used as a popular but expensive adsorbent in wastewater treatment (Jiuhui, 2008). Portlandite, gypsum, calcite, and powdered activated carbon were purchased in p.a. grade. C-S-H phases were prepared by Irbe et al. (2019) and hydrotalcite was kindly provided by Bankauskaite and Baltakys (2011). Friedel's salt was prepared by precipitation according to Balonis and Glasser (2009). For these single phase experiments 10 mg of the solid phase was added to 10 ml of Congo red solution (100 mg L^{-1} dye).

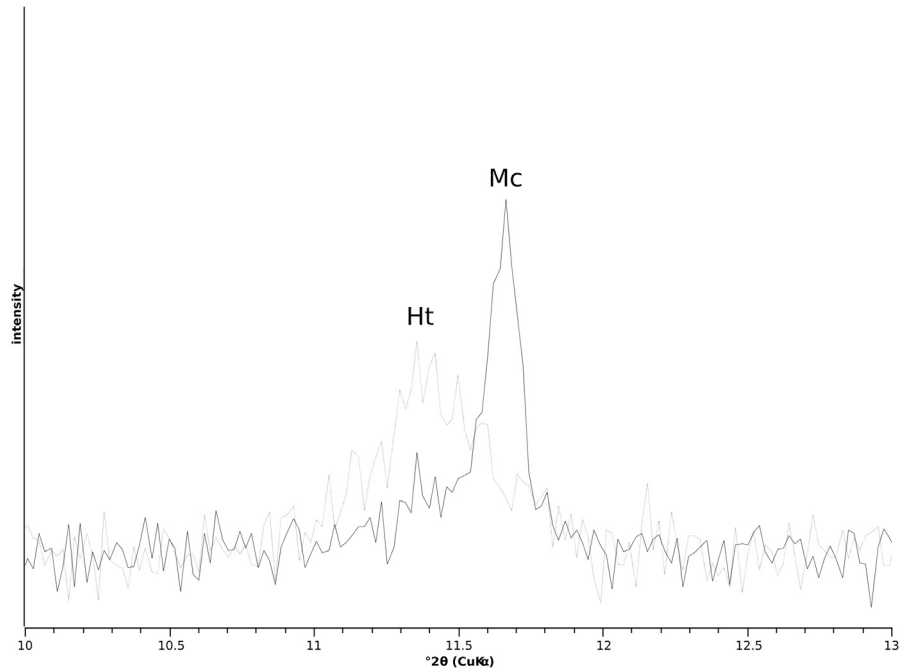

FIGURE 3 | Detail of the X-ray diffractograms of the powdered surface layers of the hardened cement paste flat prisms 65_SO (dashed line, storage in sodium sulfate solution (30 gl^{-1} SO_4^{2-}) and 65_OH (solid line, storage in saturated calcium hydroxide solution). Ht: hydrotalcite; Mc: monocarboaluminate.

3 RESULTS AND DISCUSSION

3.1 Characterization of Hardened Binder Paste Surfaces

XRD analysis showed that all the hardened binder paste surfaces contained calcite and ettringite (**Figure 2**). All hardened binder compositions also contained hydrotalcite due to the high magnesium content GGBS. For samples stored in saturated calcium hydroxide solution, monocarboaluminate instead of hydrotalcite was detected (**Figure 3**). Thus, the composition of the LDH phases being formed in hardened binder paste is likely to be controlled by the composition of the storage solution and by the chemical composition of the binder [with the Ca/Mg ratio being an important parameter (Walkley et al., 2017)], since the absence of calcium in the sodium sulfate solution could favor the formation of hydrotalcite instead of monocarboaluminate due to the decreased Ca/Mg ratio in the outermost surface layer of the flat prism after storage in sodium sulfate solution. Portlandite was found in all hardened binder paste surfaces that were stored in saturated calcium hydroxide solution, but not in the surfaces of samples stored in sodium sulfate solution. This is due to the lower pH of the latter storage solution [pH = 12.6 for the saturated calcium hydroxide solution vs. pH = 7.4 for the sodium sulfate solution (30 gl^{-1} SO_4^{2-})]. It should be noted that the amounts of powdered surface samples for X-ray analysis were limited and that the mass concentrations of the detected phases might vary in different parts of flat prisms surfaces. Therefore, no quantitative Rietveld analysis was performed on the X-ray diffraction data of the powdered surface samples. N_2-BET measurements of the specific surface area showed that the outermost 200 μm layer of hardened binder pastes with high GGBS contents stored in sodium sulfate solution has a large specific surface area (65_SO4 and 80_SO4, **Figure 1**, left). SEM images and EDS analysis of these surfaces revealed fine nanosheet-like structures that are rich in magnesium (**Figure 1**, right) and that these structures are most likely LDH phases that contain magnesium such as hydrotalcite. Chemical analysis confirmed a pronounced accumulation of magnesium in the surface layer of these samples which was produced by the storage in sodium sulfate solution (**Figure 6**). N_2-BET specific surface areas up to 66 m^2g^{-1} are reported in the literature for hydrotalcite nanosheets (Li et al., 2016) which suggests that they are an important contributor to the high specific surface area of the hardened binder surface layer for binders rich in GGBS (65_SO4 and 80_SO4). In general, the formation of a carbonated surface layer following an external sulfate ingress is typical for binders rich in GGBS (**Figure 4**), likely caused by interaction with dissolved carbon dioxide of the storage solution (Stroh et al., 2015). The rate of the formation of these carbonated surface layers is controlled by the porosity of the hardened binder paste and generally decreases with increasing GGBS content (Wagner et al., 2019). The high concentration of carbonate-containing LDH phases like hydrotalcite or monocarboaluminate in the surface layers can be explained by the high thermodynamic stability of these phases (Matschei et al., 2007; Machner et al., 2018b).

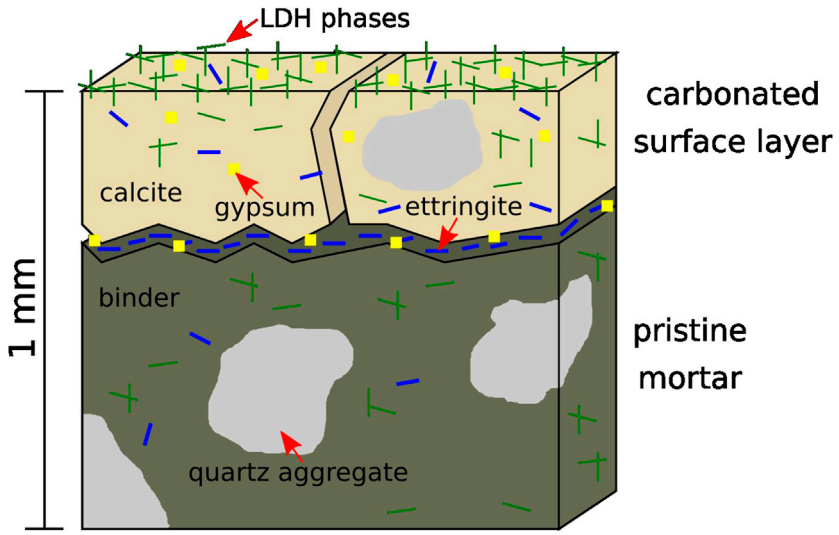

FIGURE 4 | Simplified scheme (cross section) of the outer 1 mm of a mortar based on a GGBS-rich binder after storage in a sodium sulfate solution for several months. A carbonated surface layer incorporating sulfate attack products and high concentration of LDH phases is formed.

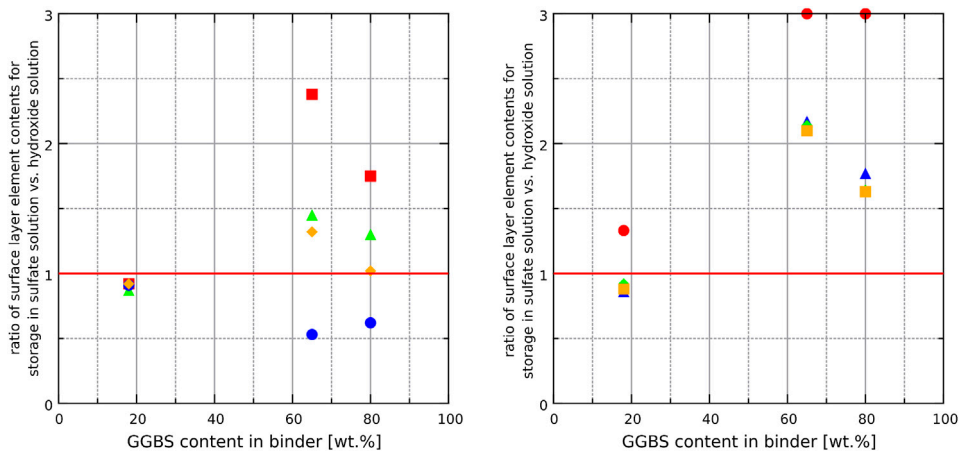

FIGURE 5 | Effect of GGBS content in the binder on the ratios of element contents (measured by ICP-OES) within the surface layer of hardened binder pastes after storage in the sodium sulfate to those of the calcium hydroxide solution. A ratio > one means that the content of an element in the surface layer is higher for storage in the sodium sulfate solution. Most minor elements are higher concentrated on binder surfaces that have been exposed to sodium sulfate solution for binders with high GGBS concentrations (65_SO4 and 80_SO4). **Left figure:** Al (▲), Mg (■), Ca (●), Si (◆). **Right figure:** Ti (▲), Ba (●), Mn (◆), Fe (■).

The chemical analysis of the hardened cement paste surfaces showed that calcium and silicon are the most abundant elements within the outermost layer of the binder since these two elements are also the main elements in the bulk binder. As expected, the content of calcium increased in samples that were stored in saturated calcium hydroxide solution since portlandite and monocarboaluminate remain stable at the samples surface. The amounts of sodium and sulfur increased in samples stored in sodium sulfate solution because ettringite (and gypsum in some cases) formed due to the sulfate ingress. Interestingly, the results also revealed that the amounts of minor elements increased considerably in the surface area of the hardened binder pastes made with large amounts of GGBS (65_SO4 and 80_SO4) and stored in sodium sulfate solution (**Figure 5**). It is likely that the diffusion of minor elements (Ti, Ba, Mn, Fe) through the pores of the hardened binder paste towards the surface is similar for both storage solutions since it is most likely based on the concentration gradient of these elements between the pore solution and the storage solution (both storage solutions were checked for contaminations of these elements in the fresh solutions). In the case of the sodium sulfate solution, minor element cations might be precipitated as insoluble sulfates at the surface. For

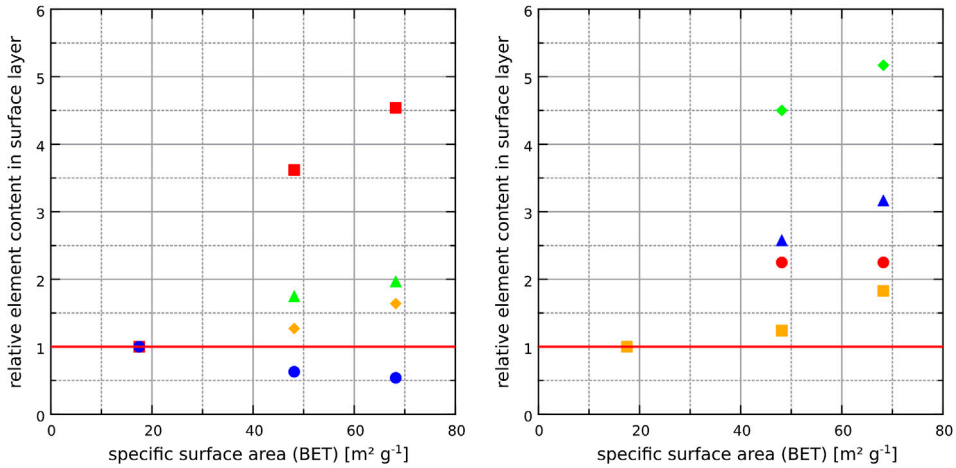

FIGURE 6 | Effect of the specific surface area of the surface layer on the relative element contents (measured by ICP-OES, wt%) for samples that were stored in the sodium sulfate solution. These values are normalized to the contents of elements for sample 18_SO4 (specific surface area (N_2-BET) of 17.5 m^2g^{-1}). The relative contents of several elements appeared to correlate with the specific surface area, indicating that they are preferably incorporated in phases with larger specific surface. Among the major elements, the effect is most prominent for magnesium, indicating the formation of Mg-rich LDH phases. For minor elements, the effect is most prominent for manganese. **Left figure:** Al (▲), Mg (■), Ca (●), Si (◆). **Right figure:** Ti (▲), Ba (●), Mn (◆), Fe (■).

example, SEM and EDS analysis revealed crystals of $BaSO_4$ scattered on the outermost surface of the samples that are based on binders rich in GGBS (**Figure 7** and **8**). The high brightness in the BSE signal and the EDS measurements show that these crystals are most likely not rich in sodium despite the storage of the sample in sodium sulfate solution [the precipitation of $BaSO_4$ from sodium sulfate solutions in the presence of barium ions can be used to synthesize barite (Dunn et al., 1999)]. In contrast, the conventional analysis of the powdered surface of the 80_SO4 prism by X-ray diffraction did not reveal barite or other phase containing barium (**Figure 2**). This indicates that the barium-containing sulfate has a mass concentration below the limit of detection of the X-ray diffraction setup since the shape of the barium-containing phase indicates a well-crystallized substance (**Figure 7**). The overall concentration of BaO in the binder of prism 80_SO4 is <0.1 wt% and it should be noted that SEM images only capture a very small part of the prism surface and that barium sulfate most likely only occurs on the outermost surface only, making it a phase that can be easily missed in bulk analysis of the hardened cement paste. This also explains why sulfates of minor elements are not usually reported in most studies on external sulfate attack on concrete when using conventional analysis approaches. In view of the present results of the chemical analysis, the amounts of minor elements in the surface layer depend on the chemical composition of the storage solution rather than on the chemical composition of the hardened binder paste in the case of binders containing sufficient amounts of GGBS. The effect of the GGBS content on the element content ratios in **Figure 5** is similar for iron, aluminum, titanium, barium and manganese. These elements are present in larger amounts in the GGBS than in the OPC used (**Table 1**). The results for phosphorus, which only occurs significantly in OPC, showed an increase in the amount of phosphorus in the surface layer of hardened binder pastes made with large amounts of GGBS after storage in the sodium sulfate solution, indicating that the GGBS content might affect the mobilization of elements originating from the OPC. The clear correlation of the element contents with the N_2-BET specific surface area of the samples in **Figure 6** indicates that the incorporation of minor elements in LDH phases could play an important role in the demobilization of these elements because the LDH system is able to incorporate chemically diverse species (Mills et al., 2012). For example, the good correlation of the accumulation of magnesium and manganese in the surface layer with the specific surface area for the samples 65_SO4 and 80_SO4 indicates the formation of Mg-Mn LDH phases (Varga et al., 2017) at the surface of GGBS-rich binders stored in sodium sulfate solution. The exact mechanism of the effect of the storage solution on the formation of LDH phases remains unclear at present and should be addressed in future research.

2.2 Exposure of Individual Phases in Hardened Binder Surfaces to Congo Red

Since the surfaces of hardened binder pastes stored in different solutions are complex mixtures of different crystalline and amorphous phases, the individual phases that typically occur in these binders were chosen for Congo red exposure experiments similar to the exposure experiments with hardened cement binder pastes described below. Powdered activated carbon was used as a benchmark substance for dye adsorption. As expected, a significant amount of Congo red is adsorbed on powdered activated carbon during the first exposure cycle. The adsorption of Congo red decreases significantly over the next three dye exposure cycles because the surface of the powdered activated carbon was saturated with adsorbed Congo red during the first exposure cycle. A similar adsorption behavior was observed for gypsum (**Figure 9**), indicating that the interaction between Congo red and gypsum surfaces is strong enough to form a stable adsorbed dye layer. This behavior is

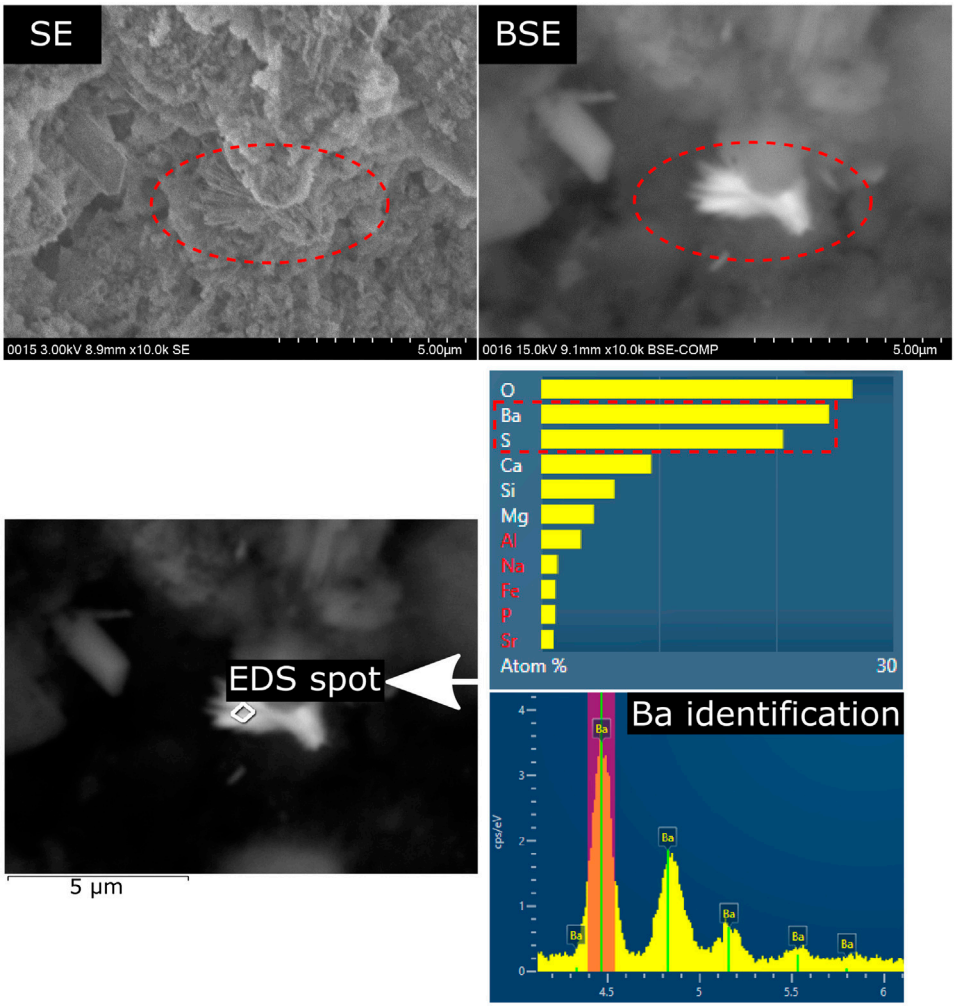

FIGURE 7 | $BaSO_4$ crystals at the outermost surface of a hardened binder paste with high GGBS content (65_SO4) following exposure to (30 gl^{-1} SO_4^{2-}). Such minor phases are not detected by conventional X-ray diffraction of bulk samples due to their low amount. They are formed at the interface between GGBS-rich binders and sodium sulfate solution and are evenly distributed on the samples surface. Low voltage SE image of the surface and high voltage BSE image of the atomic weight contrast. EDS measurements showed about equal amounts of barium and sulfur, barium was identified based on multiple energy bands to distinguish between barium and titanium.

consistent with the chemisorption of Congo red on gypsum observed by other authors (Jia et al., 2015). In contrast, calcite showed almost no removal capacity for Congo red during the first exposure cycle, but an increasing removal of Congo red from the second exposure cycle onwards, reaching up to 90 mg g^{-1} Congo red in the third and fourth exposure cycle. This behavior could be explained by restructuring effects on the calcite surface in the presence of Congo red observed by other authors who found that stable polar step edges form on which Congo red molecules can be adsorbed (Momper et al., 2015). This adsorption behavior is indirectly confirmed by the portlandite adsorption experiments. During the first exposure cycle, portlandite removed up to 95 mg g^{-1} Congo red from the aqueous solution. However, portandite is not stable against carbonation and thus calcite formed after the first exposure cycle due to carbonation by atmospheric carbon dioxide during drying. The calcite formation was confirmed by X-ray diffraction. Similar to the first exposure cycle with calcite, almost no Congo red is removed in the second exposure cycle of portlandite because fresh calcite was present in the sample at this stage. The removal of Congo red reaches up to 93 mg g^{-1} of Congo red in the forth exposure cycle which corresponds to that of pure calcite. It appears that an assumed ongoing restructuring of the surface of the newly formed calcite generates adsorption capacity for Congo red. The LDH phases hydrotalcite and Friedel's salt removed significant amounts of Congo red from the aqueous solution over all four dye exposure cycles (**Figure 9**, left). This could be explained by the ongoing substitution of the interlayer ions (CO_3^{2-} in hydrotalcite and Cl^- in Friedel's salt) with Congo red, similar to the adsorption of other azo dye anions in LDH phases reported by other authors (Darmograi et al., 2015; Li et al., 2016). The C-S-H sample also showed a high removal capacity of up to

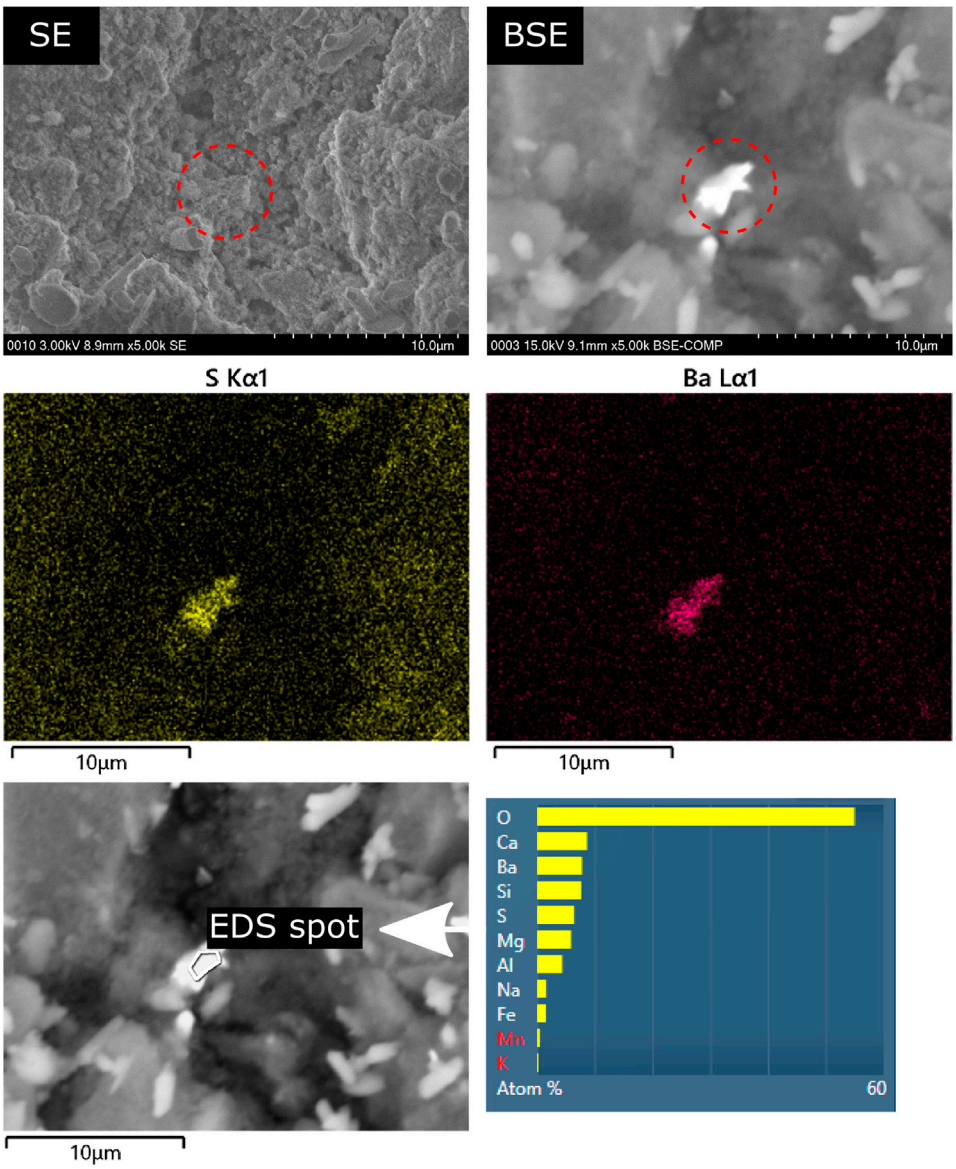

FIGURE 8 | $BaSO_4$ crystals near the outermost surface of a hardened binder paste with high GGBS content (65_SO4) following exposure to (30 gl^{-1} SO_4^{2-}), obstructed by a thin layer of binder. The $BaSO_4$ crystals are unlikely drying artifacts since they are partially or completely incorporated in the outer binder. Low voltage SE image of the surface and high voltage BSE image of the atomic weight contrast. EDS mappings of sulfur and barium reveal a local concentration maximum of these elements. EDS measurements showed about equal amounts of barium and sulfur.

105 $mg\,g^{-1}$ Congo red which corresponds to the high adsorption capacity of C-S-H for larger organic molecules because of its large specific surface area (Zhu and Sham, 2014). The small decrease in dye removal in the second exposure cycle and the increase in capacity during in the third and forth exposure cycles could, as in the case of portlandite, be due to the formation of small amounts of calcite by carbonation of the sample. Thus, the carbonation of portlandite as well as the formation of LDH phases that steadily occurs when the hardened cement paste is exposed to industrial wastewater, could increase the reusability of hardened cement paste as a substrate for removing azo dyes.

3.3 Exposure of Hardened Binder Paste Surfaces to Congo Red

The Congo red exposure experiments with hardened binder paste samples (200 µm surface layer) revealed a large degree of Congo red removal from the solution with respect to the mass of the hardened binder paste samples previously stored in sodium sulfate solution and containing large amounts of GGBS (65_SO4 and 80_SO4, **Figure 10**, left). This behavior was expected because 65_SO4 and 80_SO4 have a larger specific surface area than the other samples (**Figure 1**). However, the mass of Congo red removed from the solution for 65_SO4 was almost twice that of 80_SO4

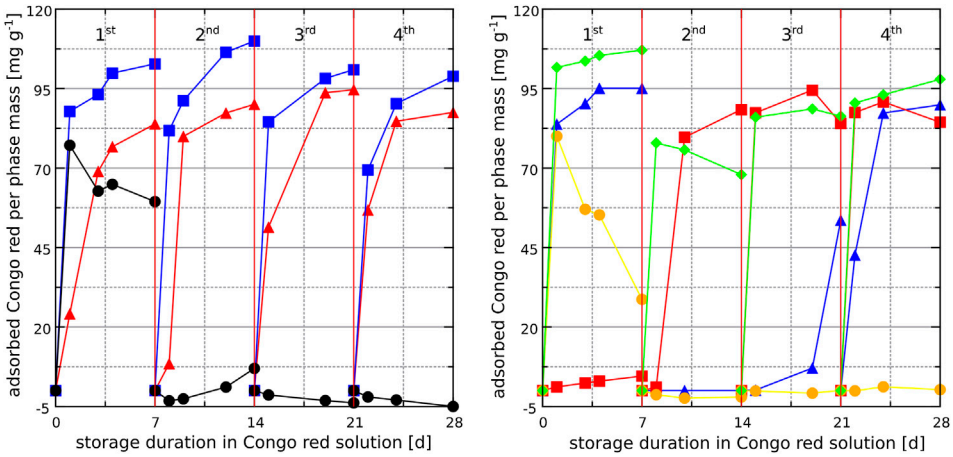

FIGURE 9 | Removal of Congo red from aqueous solutions in contact with different individual phases, based on photometry results for four consecutive exposure cycles. **Left:** hydrotalcite (▲), Friedel's salt (■) and powdered activated carbon (●). **Right:** portlandite (▲), calcite (■), gypsum (●) and calcium silicate hydrates (C-S-H) (◆).

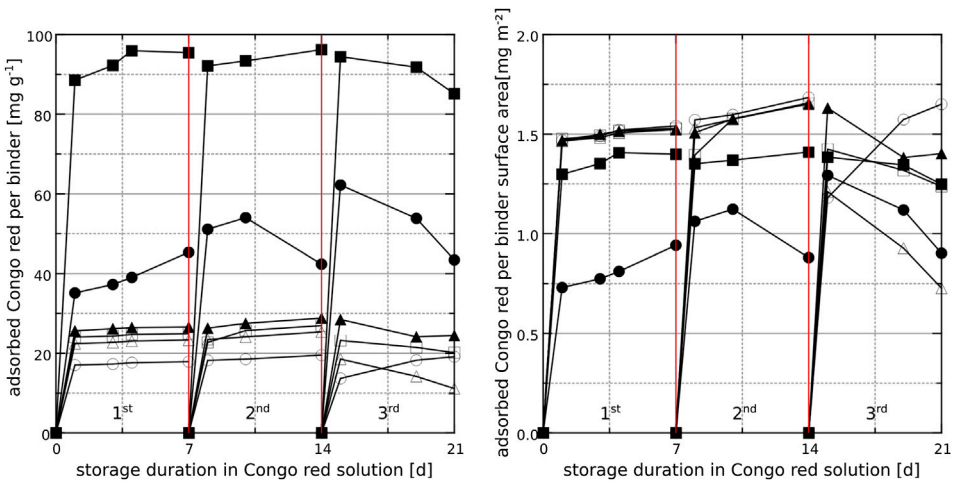

FIGURE 10 | Removal of Congo red from aqueous solutions in contact with hardened binder paste surfaces (powder of 200 µm surface layer), based on photometry results for three consecutive exposure cycles. **Left:** removed Congo red per mass of hardened binder paste. **Right:** removed Congo red per specific surface area of hardened cement paste. 18_SO4 (▲), 65_SO4 (■) and 80_SO4 (●). The open symbols are for samples with the same binder composition, but which were stored in saturated calcium hydroxide solution before the dye exposure experiments.

although the specific surface area ratio of the two samples 65_SO4/80_SO4 is 1.4. The removal of Congo red with respect to specific surface area of the binders is also larger for 65_SO4 than for 80_SO4 (**Figure 10**, right). When considering the removed mass of Congo red with respect to the specific surface area of the hardened binder surface, the dye removal ability of GGBS-rich binders after storage in the sodium sulfate solution is lower than that after storage in the calcium hydroxide solution (**Figure 10**, right). This could be caused by the differences in the phase assemblage in the binder surfaces which depends on the pre-storage solution. It is also possible that SO_4^{2-} competes with Congo red for adsorption as an interlayer ion in the LDH phases (Darmograi et al., 2016). In general, the decrease in the extinction at λ = 498 nm was equal to the decrease in the extinction at λ = 340 nm as expected for the removal of Congo red from the aqueous solutions. The overall correlation of specific surface area and Congo red removal suggests, on first sight, that adsorption is primarily responsible for the decrease in dye concentration. However in this case, a decrease in the dye removal over all three exposure cycles would be expected, which was not observed for this setup. The pH of the dye solution remained stable at around pH = 10 for all samples during all three exposure cycles, thus excluding variations in the phase assemblage due to pH changes. In addition to the results shown for individual phases in **Figure 9** the removal capacity

of barite was also investigated and found to be very low (9 mg g^{-1} in the first exposure cycle, no dye removal in the following cycles), indicating that the barite crystals observed on surfaces of GGBS-rich binders stored in sodium sulfate solution (65_SO4 and 80_SO4, 7) do not significantly contribute to the good overall Congo red removal ability of these samples.

4 CONCLUSION

This study provides a link between azo dye wastewater treatment and cement chemistry. The mineralogical and chemical composition of the outermost layer of hardened binder paste is a function of both the chemical composition of the binder and the chemical composition of the storage solution. Though this appears to be an obvious result from a chemical point of view, it is emphasized that this knowledge should be considered in concrete design by choosing a binder that produces the desired surface phases on contact of the concrete structural component with wastewater of known chemical composition. Storage in sodium sulfate solution lead to the formation of hydrotalcite nanosheets on the surfaces of hardened binder pastes rich in magnesium provided by the GGBS and these nanosheets resulted in a large specific surface area of the binder surface. Sodium sulfate solution also appeared to intensify the precipitation of minor element sulfates at the surface of the hardened binder, thus significantly increasing the amounts of these elements (manganese, barium, titanium) at the surface compared to the bulk sample. The LDH phases hydrotalcite and Friedel's salt as well as C-S-H phases exhibit a high removal capacity for Congo red over a number of dye exposure cycles. The removal capacity of these phases is higher than that of powdered activated carbon or gypsum. The results also suggest that the removal of Congo red from aqueous solutions in contact with hardened cementitious binders could be delayed owing to the effect of carbonation and, possibly, also due to surface restructuring of calcite in the surface layer of the hardened binder.

The results showed that the surfaces of GGBS-rich binders that were previously stored in a sodium sulfate solution (30 gl^{-1} SO_4^{2-}) exhibit an increased overall removal capacity for Congo red over multiple dye exposure cycles compared to binders with low GGBS contents or binders that were stored in calcium hydroxide solution. This suggests that binders that are rich in GGBS (and thus rich in magnesium) could contribute to the removal of azo dyes from industrial wastewater if the chemical composition of the wastewater supports the formation of phases with high specific surface area at the surface of the hardened binder paste. Further investigation is required to assess the detailed relationship between wastewater composition and the phase assemblage in outermost layer of the surfaces of hardened binder pastes of different chemical and mineralogical composition. A future application of this concept requires detailed investigations on the adsorption parameters of the most promising binder compositions.

This knowledge could lead to the improvement of guidelines concerning the usage of specific binders in structures for wastewater storage or treatment. Furthermore, the observation that cementitious binders with certain chemical compositions could act as a substrate for the removal of azo dyes from industrial wastewater could provide a low-cost contribution to wastewater treatment and would be an economically attractive treatment method for the textile industry, especially for developing and newly industrialized countries.

DATA AVAILABILITY STATEMENT

The raw data supporting the conclusions of this article will be made available by the authors, without undue reservation.

AUTHOR CONTRIBUTIONS

MW, CE, and DH contributed to the conceptualization. MW, CE, HH, and DH contributed to the methodology. CE and MW contributed to the investigation. MW and CE prepared the original draft. The draft was reviewed and edited by MW, CE, BH, HH, and DH. DH, HH, and BH supervised the project. All authors have agreed to the published version of the article.

FUNDING

This work was supported by the German Research Foundation (DFG) and the Technical University of Munich (TUM) in the framework of the Open Access Publishing Program.

ACKNOWLEDGMENTS

The authors thank L. Irbe for providing samples of C-S-H-phases and K. Baltakys for providing the hydrotalcite samples.

REFERENCES

Adeleke, J. T., Theivasanthi, T., Thiruppathi, M., Swaminathan, M., Akomolafe, T., and Alabi, A. B. (2018). Photocatalytic degradation of methylene blue by zno/nife2o4 nanoparticles. *Appl. Surf. Sci.* 455, 195–200. doi:10.1016/j.apsusc.2018.05.184

Balonis, M., and Glasser, F. P. (2009). The density of cement phases. *Cem. Concr. Res.* 39, 733–739. doi:10.1016/j.cemconres.2009.06.005

Banat, I. M., Nigam, P., Singh, D., and Marchant, R. (1996). Microbial decolorization of textile-dyecontaining effluents: a review. *Bioresour. Technol.* 58, 217–227. doi:10.1016/s0960-8524(96)00113-7

Bankauskaite, A., and Baltakys, K. (2011). The hydrothermal synthesis of hydrotalcite by using different partially soluble and insoluble in water mangesium and aluminium components. *Sci. Sinter.* 43, 261–275. doi:10.2298/sos1103261b

Camacho, L., Dumée, L., Zhang, J., Li, J.-d., Duke, M., Gomez, J., et al. (2013). Advances in membrane distillation for water desalination and purification applications. *Water* 5, 94–196. doi:10.3390/w5010094

Darmograi, G., Prelot, B., Geneste, A., Martin-Gassin, G., Salles, F., and Zajac, J. (2016). How does competition between anionic pollutants affect adsorption onto mg-al layered double hydroxide? three competition schemes. *J. Phys. Chem. C* 120, 10410–10418. doi:10.1021/acs.jpcc.6b01888

Darmograi, G., Prelot, B., Layrac, G., Tichit, D., Martin-Gassin, G., Salles, F., et al. (2015). Study of adsorption and intercalation of orange-type dyes into Mg-Al layered double hydroxide. *J. Phys. Chem. C* 119, 23388–23397. doi:10.1021/acs.jpcc.5b05510

Debecker, D. P., Gaigneaux, E. M., and Busca, G. (2009). Exploring, tuning, and exploiting the basicity of hydrotalcites for applications in heterogeneous catalysis. *Chem. Eur J.* 15, 3920–3935. doi:10.1002/chem.200900060

DIN (2011). *DIN EN 197-1:2011: zement - Teil 1: zusammensetzung, Anforderungen und KonformitÃ¤tskriterien von Normalzement (English: cement - Part 1: composition, specifications and conformity criteria for common cements)*. (Berlin, Germany: Beuth Verlag).

Dos Santos, A. B., Cervantes, F. J., and Van Lier, J. B. (2007). Review paper on current technologies for decolourisation of textile wastewaters: perspectives for anaerobic biotechnology. *Bioresour. Technol.* 98, 2369–2385. doi:10.1016/j.biortech.2006.11.013

Dunn, K., Daniel, E., Shuler, P. J., Chen, H. J., Tang, Y., and Yen, T. F. (1999). Mechanisms of surface precipitation and dissolution of barite: a morphology approach. *J. Colloid Interface Sci.* 214, 427–437. doi:10.1006/jcis.1999.6224

Georgiou, D., and Aivasidis, A. (2006). Decoloration of textile wastewater by means of a fluidized-bed loop reactor and immobilized anaerobic bacteria. *J. Hazard Mater.* 135, 372–377. doi:10.1016/j.jhazmat.2005.11.081

Gong, K., and White, C. E. (2016). Impact of chemical variability of ground granulated blast-furnace slag on the phase formation in alkali-activated slag pastes. *Cem. Concr. Res.* 89, 310–319. doi:10.1016/j.cemconres.2016.09.003

Habert, G., Billard, C., Rossi, P., Chen, C., and Roussel, N. (2010). Cement production technology improvement compared to factor 4 objectives. *Cem. Concr. Res.* 40, 820–826. doi:10.1016/j.cemconres.2009.09.031

Huang, P.-P., Cao, C.-Y., Wei, F., Sun, Y.-B., and Song, W.-G. (2015). Mgal layered double hydroxides with chloride and carbonate ions as interlayer anions for removal of arsenic and fluoride ions in water. *RSC Adv.* 5, 10412–10417. doi:10.1039/c4ra15160g

Imtiazuddin, S. M. (2018). Impact of textile wastewater pollution on the environment. *Pakistan Text. J.* 8, 38–39. doi:10.3844/ajessp.2007

Irbe, L., Beddoe, R. E., and Heinz, D. (2019). The role of aluminium in c-a-s-h during sulfate attack on concrete. *Cem. Concr. Res.* 116, 71–80. doi:10.1016/j.cemconres.2018.11.012

Jia, X.-J., Wang, J., Wu, J., Du, Y., Zhao, B., and Engelsen, D. d. (2015). Bouquet-like calcium sulfate dihydrate: a highly efficient adsorbent for Congo red dye. *RSC Adv.* 5, 72321–72330. doi:10.1039/c5ra11514k

Jiuhui, Q. U. (2008). Research progress of novel adsorption processes in waterpurification: a review. *J. Environ. Sci.* 20, 1–13. doi:10.1016/S1001-0742(08)60001-7

Juenger, M. C. G., and Siddique, R. (2015). Recent advances in understanding the role of supplementary cementitious materials in concrete. *Cem. Concr. Res.* 78 (Part A), 71–80. doi:10.1016/j.cemconres.2015.03.018

Kant, R. (2012). Textile dyeing industry an environmental hazard. *Nat. Sci.* 4, 22–26. doi:10.4236/ns.2012.41004

Li, J., Cui, H., Song, X., Zhang, G., Wang, X., Song, Q., et al. (2016). Adsorption and intercalation of organic pollutants and heavy metal ions into mgal-ldhs nanosheets with high capacity. *RSC Adv.* 6, 92402–92410. doi:10.1039/c6ra18783h

Li, Y., Zhang, J., Zhang, Y., and Quan, X. (2017). Scaling-up of a zero valent iron packed anaerobic reactor for textile dye wastewater treatment: a potential technology for on-site upgrading and rebuilding of traditional anaerobic wastewater treatment plant. *Water Sci. Technol.* 76, 823–831. doi:10.2166/wst.2017.270

Lin, P.-J., Yang, M.-C., Li, Y.-L., and Chen, J.-H. (2015). Prevention of surfactant wetting with agarose hydrogel layer for direct contact membrane distillation used in dyeing wastewater treatment. *J. Membr. Sci.* 475, 511–520. doi:10.1016/j.memsci.2014.11.001

Ma, B., Fernandez-Martinez, A., Grangeon, S., Tournassat, C., Findling, N., Carrero, S., et al. (2018). Selenite uptake by ca-al ldh: a description of intercalated anion coordination geometries. *Environ. Sci. Technol.* 52, 1624–1632. doi:10.1021/acs.est.7b04644

Machner, A., Zajac, M., Ben Haha, M., Kjellsen, K. O., Geiker, M. R., and De Weerdt, K. (2018a). Limitations of the hydrotalcite formation in portland composite cement pastes containing dolomite and metakaolin. *Cem. Concr. Res.* 105, 1–17. doi:10.1016/j.cemconres.2017.11.007

Machner, A., Zajac, M., Ben Haha, M., Kjellsen, K. O., Geiker, M. R., and De Weerdt, K. (2018b). Stability of the hydrate phase assemblage in portland composite cements containing dolomite and metakaolin after leaching, carbonation, and chloride exposure. *Cem. Concr. Compos.* 89, 89–106. doi:10.1016/j.cemconcomp.2018.02.013

Matschei, T., Lothenbach, B., and Glasser, F. P. (2007). The afm phase in portland cement. *Cem. Concr. Res.* 37, 118–130. doi:10.1016/j.cemconres.2006.10.010

Mills, S. J., Christy, A. G., Génin, J.-M. R., Kameda, T., and Colombo, F. (2012). Nomenclature of the hydrotalcite supergroup: natural layered double hydroxides. *Mineral. Mag.* 76, 1289–1336. doi:10.1180/minmag.2012.076.5.10

Mohan, S. V., Rao, N. C., and Sarma, P. N. (2007). Simulated acid azo dye (acid black 210) wastewater treatment by periodic discontinuous batch mode operation under anoxic-aerobic-anoxic microenvironment conditions. *Ecol. Eng.* 31, 242–250. doi:10.1016/j.ecoleng.2007.07.003

Mohapatra, L., and Parida, K. (2016). A review on the recent progress, challenges and perspective of layered double hydroxides as promising photocatalysts. *J. Mater. Chem.* 4, 10744–10766. doi:10.1039/c6ta01668e

Momper, R., Nalbach, M., Lichtenstein, K., Bechstein, R., and Kühnle, A. (2015). Stabilization of polar step edges on calcite (10.4) by the adsorption of Congo red. *Langmuir* 31, 7283–7287. doi:10.1021/acs.langmuir.5b01043

Morimoto, K., Tamura, K., Iyi, N., Ye, J., and Yamada, H. (2011). Adsorption and photodegradation properties of anionic dyes by layered double hydroxides. *J. Phys. Chem. Solid.* 72, 1037–1045. doi:10.1016/j.jpcs.2011.05.018

Saleh, R., and Taufik, A. (2019). Degradation of methylene blue and Congo-red dyes using fenton, photo-fenton, sono-fenton, and sonophoto-fenton methods in the presence of iron(ii,iii) oxide/zinc oxide/graphene (fe3o4/zno/graphene) composites. *Separ. Purif. Technol.* 210, 563–573. doi:10.1016/j.seppur.2018.08.030

Sarayu, K., and Sandhya, S. (2012). Current technologies for biological treatment of textile wastewater-A review. *Appl. Biochem. Biotechnol.* 167, 645–661. doi:10.1007/s12010-012-9716-6

Shan, R.-r., Yan, L.-g., Yang, Y.-m., Yang, K., Yu, S.-j., Yu, H.-q., et al. (2015). Highly efficient removal of three red dyes by adsorption onto mg-al-layered double hydroxide. *J. Ind. Eng. Chem.* 21, 561–568. doi:10.1016/j.jiec.2014.03.019

Shetti, N. P., Malode, S. J., Malladi, R. S., Nargund, S. L., Shukla, S. S., and Aminabhavi, T. M. (2019). Electrochemical detection and degradation of textile dye Congo red at graphene oxide modified electrode. *Microchem. J.* 146, 387–392. doi:10.1016/j.microc.2019.01.033

Soltani, Z., Salavati, H., Movahedi, M., and Sadeghi, Z. (2018). Mgcafe- layered double hydroxides (ldh) for Congo red dye removal in aqueous solution. *Iran. Chem. Commun.* 6, 39–48

Stroh, J., Meng, B., and Emmerling, F. (2015). Monitoring of sulphate attack on hardened cement paste studied by synchrotron xrd. *Solid State Sci.* 48, 278–285. doi:10.1016/j.solidstatesciences.2015.08.006

Taylor, H. F. W. (1973). Crystal structures of some double hydroxide minerals. *Mineral. Mag.* 39, 377–389. doi:10.1180/minmag.1973.039.304.01

Tichit, D., Lhouty, M. H., Guida, A., Chiche, B. H., Figueras, F., Auroux, A., et al. (1995). Textural properties and catalytic activity of hydrotalcites. *J. Catal.* 151, 50–59. doi:10.1006/jcat.1995.1007

Van der Zee, F. P., Lettinga, G., and Field, J. A. (2001). Azo dye decolourisation by anaerobic granular sludge. *Chemosphere* 44, 1169–1176. doi:10.1016/s0045-6535(00)00270-8

Varga, G., Muráth, S., Ujvári, L., Kukovecz, Á., Kónya, Z., Sipos, P., et al. (2017). Mn(ii)-containing layered double hydroxide composites: synthesis, characterization and an application in ullmann diaryl etherification. *React. Kinet. Mech. Catal.* 121, 175–184. doi:10.1007/s11144-016-1127-1

Wagner, M., Decker, M., Zausinger, C., Beddoe, R. E., and Heinz, D. (2019). "External sulfate attack on hardened opc-ggbs binders: from chemical composition and sample geometry towards numerical modeling of construction component behavior," in 15th international congress on the chemistry of cement, Prague, Czech Republic, September 16–20, 2019.

Walkley, B., San Nicolas, R., Sani, M.-A., Bernal, S. A., van Deventer, J. S. J., and Provis, J. L. (2017). Structural evolution of synthetic alkali-activated CaO-MgO-Na 2 O-Al 2 O 3 -SiO 2 materials is influenced by Mg content. *Cem. Concr. Res.* 99, 155–171. doi:10.1016/j.cemconres.2017.05.006

Wang, X., Gu, X., Lin, D., Dong, F., and Wan, X. (2007). Treatment of acid rose dye containing wastewater by ozonizing - biological aerated filter. *Dyes Pigm.* 74, 736–740. doi:10.1016/j.dyepig.2006.05.009

Weisburger, J. H. (2002). Comments on the history and importance of aromatic and heterocyclic amines in public health. *Mutat. Res. Fund Mol. Mech. Mutagen* 506–507, 9–20. doi:10.1016/s0027-5107(02)00147-1

Yang, Z., Wang, F., Zhang, C., Zeng, G., Tan, X., Yu, Z., et al. (2016). Utilization of ldh-based materials as potential adsorbents and photocatalysts for the decontamination of dyes wastewater: a review. *RSC Adv.* 6, 79415–79436. doi:10.1039/c6ra12727d

Zhang, B., Dong, Z., Sun, D., Wu, T., and Li, Y. (2017). Enhanced adsorption capacity of dyes by surfactant-modified layered double hydroxides from aqueous solution. *J. Ind. Eng. Chem.* 49, 208–218. doi:10.1016/j.jiec.2017.01.029

Zhang, Y. J., and Chai, Q. (2014). Alkali-activated blast furnace slag-based nanomaterial as a novel catalyst for synthesis of hydrogen fuel. *Fuel* 115, 84–87. doi:10.1016/j.fuel.2013.06.051

Zhang, Y. J., Liu, L. C., Ni, L. L., and Wang, B. L. (2013). A facile and low-cost synthesis of granulated blast furnace slag-based cementitious material coupled with fe2o3 catalyst for treatment of dye wastewater. *Appl. Catal. B Environ.* 138-139, 9–16. doi:10.1016/j.apcatb.2013.02.025

Zhu, H.-Y., Jiang, R., Huang, S.-H., Yao, J., Fu, F.-Q., and Li, J.-B. (2015). Novel magnetic nife2o4/multi-walled carbon nanotubes hybrids: facile synthesis, characterization, and application to the treatment of dyeing wastewater. *Ceram. Int.* 41, 11625–11631. doi:10.1016/j.ceramint.2015.05.122

Zhu, Y.-J., and Sham, T.-K. (2014). The potential of calcium silicate hydrate as a carrier of ibuprofen. *Expet Opin. Drug Deliv.* 11, 1337–1342. doi:10.1517/17425247.2014.923399

Conflict of Interest: The authors declare that the research was conducted in the absence of any commercial or financial relationships that could be construed as a potential conflict of interest.